



# Synthesis, antimicrobial activity, theoretical investigation, and electrochemical studies of cellulosic metal complexes

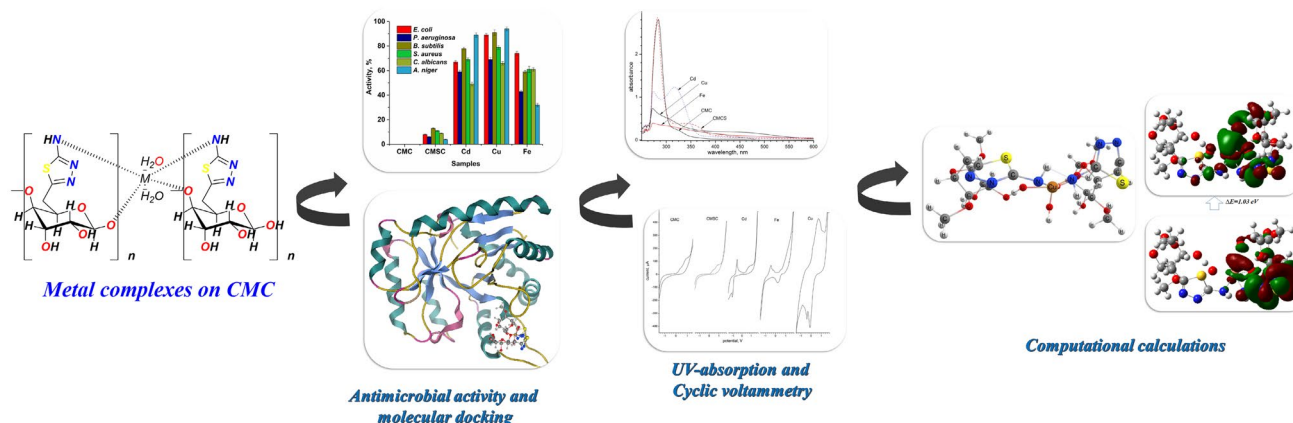
Asmaa M. Fahim<sup>1</sup> · Mohamed Hasanin<sup>2</sup> · I. H. I. Habib<sup>3</sup> · Rehab O. El-Attar<sup>3</sup> · Sawsan Dacroy<sup>2</sup>

Received: 25 October 2022 / Accepted: 19 March 2023 / Published online: 10 April 2023  
© Iranian Chemical Society 2023

## Abstract

In this explanation, we explained how to make 5-amino-1,3,4-thiadiazol cellulose by reacting carboxymethyl cellulose (CMC) with thiosemicarbazide and undergoing intermolecular cyclization in the presence of acid medium (2R,3R,4S,5R,6R). This was confirmed by spectral analysis to be -6-(((5-amino-1,3,4-thiadiazol-2-yl)methyl)-2,5-dimethoxytetrahydro-2H-pyran-3,4-diol (CMSC) (4). Moreover, the 1,3,4-thiazole cellulose 4 reacts with the ligand metal chlorides at a ratio of 1:2 to produce the corresponding new metal complexes. Additionally, the obtained complexes were examined using FT-IR, SEM, TGA, and UV spectroscopy, which demonstrated that the chelation of the amino group of the thiadiazole with the OH of the CMC and the presence of Cd(II), Cu(II), and Fe(III) completely altered the morphology of the CMC fibers, resulting in tiny needles on the surface and coating most of the CMC. Additionally, these complexes were shown to have antimicrobial properties, with the Cu(II) complex cellulose demonstrating excellent antimicrobial activity in comparison with other complexes. It was also demonstrated through docking with various proteins, including (PDB ID:3t88), (PDB ID:2wje), (PDB ID:4ynt), (PDB ID:1tgh), that the Cu(II) complex was more stable than other complexes. Using cyclic voltammetry, the surface oxidation and reduction of these complexes as well as their capacity for reactivity were verified. Also, these complexes' physical descriptors were explained to determine their reactivity using the DFT/B3PW91/LANDZ2 basis set.

## Graphical Abstract



**Keywords** Cellulose metal complexes · Antimicrobial activity · Docking investigation · Cyclic voltammetry · Computational studies

✉ Asmaa M. Fahim  
asmaamahmoud8521@gmail.com;  
am.abdel-wahid@nrc.sci.eg

Extended author information available on the last page of the article

## Introduction

Considering that agricultural waste is one of the primary sources of recyclable materials, management of this waste is a major challenge. The majority of researchers have recently focused their attention on cellulosic components in this agricultural waste [1, 2]. The use of cellulosic materials continues to increase due to their distinctive structure, non-toxic, biodegradable, biocompatibility, and capacity to form more hydrogen bonds, which makes them more reactive [3, 4]. Industry uses for cellulose moiety include environmentally friendly conductive materials that can be utilized as replacement materials in a variety of applications [5, 6]. The most widely used cellulose derivative is carboxymethyl cellulose (CMC) due to the presence of 1, 4-glycosidic linkages, which reduce cellulose's viscosity and make its surface more thickening and emulsifying, it has great chemical interaction ability [7, 8]. When the release of metals occurs within a tied range, complex-based biopolymers are employed in biological systems with a high safety profile. Biopolymers are also listed as the highest-safety polymers for biological systems [9, 10]. Moreover, the presence of metal compounds on the surface of the cellulosic fabric increases intramolecular hydrogen interactions, which can lead to an increase in the aggregation of bacterial cells on the fabric's surface and an increase in the active sites' antimicrobial effectiveness [11, 12], and the docking relationship supports the metals' interaction with the surface of the cellulose [13, 14]. Also, the biological activity of cellulose in pharmaceutical applications and the most important drug in medication used to treat cancer is Bleomycin (I), also Clindamycin (II) which used for antibiotic for treatment of a number of bacterial infections, as displayed in Fig. 1.

In this case, an electron will be excited from the highest occupied molecular orbital (HOMO) to the lowest unoccupied molecular orbital (LUMO) due to optical or electrical

processes, creating a hole in the HOMO. The LUMO is the energy required to take electrons into a molecule, meaning a reduction process, while the HOMO indicates the energy required to lose electrons from a molecule, which is an oxidation process. The energy band gap is the name given to the potential difference between these levels ( $E_g$ ) for researching novel synthetic organic materials that show promise for use in organic light-emitting diodes in real-time (OLED) [15], organic solar cells (OSC) [16], and organic field-effect transistors (OFET) [17]. The HOMO and LUMO energy levels as well as the energy band gap between them must be understood. Electrochemical measurements can quickly reach these energy level positions. In addition, the electrochemical behaviors demonstrated cyclic voltammetry (CV) to determine their electrocatalytic activity as well as their electron transfer to determine their HOMO–LUMO of the ligands and chelate [18]. Aqueous media and the presence of electrically conductive substances, such as tetra butyl ammonium salts, were traditionally used while conducting cyclic voltammetry. This method, however, has significant drawbacks, including the need for an overnight drying process to remove trace water and the need for a solvent distillation under vacuum to remove electroactive organic interference. Additionally, passing nitrogen gas through the process to remove dissolved oxygen from the solvents can also result in air pollution that is toxic or hazardous to human health and/or the environment. Moreover, an internal organic solvent-containing reference electrode made of Ag/AgCl must be prepared. Moreover, some organic compounds, particularly those with lengthy chains of polymers, are scarcely soluble in organic solvents. A newly developed alternative method, which is now being investigated with additional information and preparation for a separate publication, can easily eliminate all these flaws [19, 20]. As shown by the results below, this method involves fabricating carbon paste electrodes that have been changed with the organic

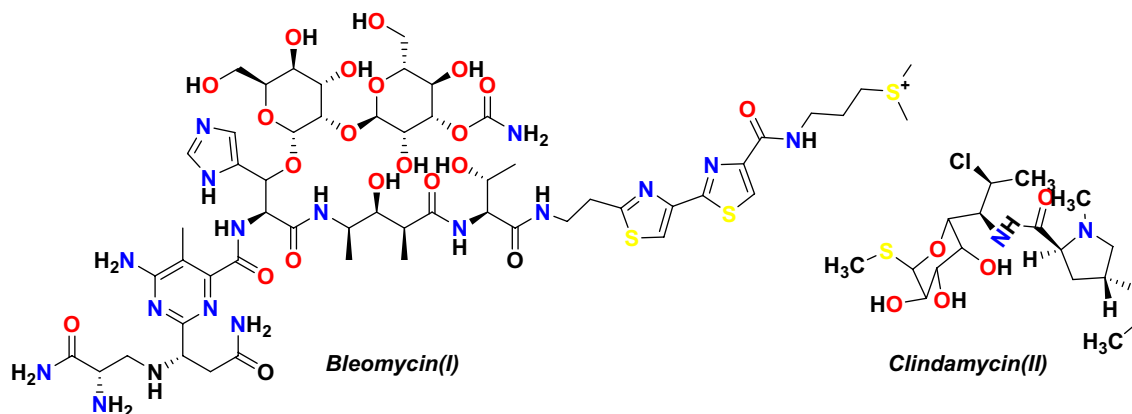


Fig. 1 Some drugs containing cellulose moiety

compounds under investigation and measuring the oxidation and reduction potentials in aqueous solutions.

Using carboxymethyl cellulose (CMC) and thiosemicarbazide as catalysts, we created novel 5-amino-1,3,4-thiadiazol cellulose (CMSC) in this study, which was then verified using spectral analysis. Through investigation using SEM, FT-IR, and TGA analysis, the chemical characterization of CMSC, which includes NH<sub>2</sub> and the OH of cellulose, gave the capacity to interact effectively with metals like Cu(II), Cd(II), and Fe(III) and proved their stabilities. Particularly, cellulosic Cu(II) complex, tightly accumulated on the surface of cellulose and made more hydrogen bonding interactions that were confirmed via docking stimulation, electrochemical analysis, and computational studies using the DFT/ B3PW91/LANDZ2 basis set and confirmed their stabilities; metal complexes were found to have high antimicrobial evaluation [21, 22].

## Materials and methods

### Instruments

The Shimadzu FT-IR 8101 PC infrared spectrophotometer was used to explore the FT-IR. Images were produced using an accelerating voltage of 10–15 kV. The <sup>1</sup>H NMR spectra were determined in DMSO-d<sub>6</sub> at 300 MHz on a Varian Mercury VX 300 NMR spectrometer using trimethyl silane as an internal typical, and scanning electron microscopes (SEM) were investigated using the JEOL JXA-840A electron probe microanalyzer firm. Using a heating rate of 10°C/min, a TGA Perkin-Elmer (STA6000) was used to test the thermal stability of films. Under an environment of air, the temperature ranged from ambient temperature to 900 °C. On a Diano X-ray diffractometer with a CoK radiation source energized at 45 kV and a Philips X-ray diffractometer (PW 1930 generator, PW 1820 goniometer) with a CuK radiation source (wavelength = 0.15418 nm), the XRD patterns were examined in the reflection mode at a diffraction angle range of 2° from 10° to 70°.

### Materials and reagents

Carboxymethyl cellulose (CMC), thiosemicarbazide, (CuCl<sub>2</sub>·2H<sub>2</sub>O), (CdCl<sub>2</sub>·2H<sub>2</sub>O), and (FeCl<sub>3</sub>·6H<sub>2</sub>O) were purchased from Sigma Aldrich, USA. All chemicals were used as received without further treatment. The reagents and microbial media were of analytical grade and used without any previous treatment.

## Methods of synthesis

### Synthesis of (2R,3R,4S,5R,6R)-6-((5-amino-1,3,4-thiadiazol-2-yl)methyl)-2,5-dimethoxytetrahydro-2H-pyran-3,4-diol(CMSC) (4)

Thiosemicarbazide (0.09 g, 1 mmol) and carboxymethyl cellulose (CMC) (0.2 g, 1 mmol) were dissolved in 40 ml of distilled water with constant stirring, and pH was adjusted to 3 using HCl. The reaction was refluxed for 1 h, and the results were detected using TLC using diluted NH<sub>3</sub>, the acidic reaction media was neutralized to a pH of 6. After neutralization, the oily portion was separated from the watery layer that had developed. The leftover oily portion was treated with ether to solidify it. The resultant solid was then refined and filtered using the appropriate solvent to allow recrystallization (2R,3R,4R,5R,6R) Six-(((5-amino-1,3,4-thiadiazol-2-yl)methyl)tetrahydro-2H-pyran-2,3,4,5-tetraol (CMSC)(4): (grey solid); yield(88%) at m.p.=235°; IR (KBr)  $\nu_{\max}/\text{cm}^{-1}$ : 3877 (OH), 3456 (NH<sub>2</sub>) and its <sup>1</sup>H NMR (DMSO-d<sub>6</sub>,  $\delta$  ppm): 2.40 (m, 2H, H<sub>2</sub>C), 3.61 (m, 2H, HC), 4.39 (m, 2H, HC), 5.00 (t, 2H, HC), 5.02 (m, 1H, HO-exchangeable), 5.08 (d, 1H, HO-exchangeable), 6.39 (m, 2H, NH<sub>2</sub>-exchangeable), MS (*m/z*): 291 ((M-H)<sup>+</sup>, 100.0%), (Anal.Calcd. for C<sub>10</sub>H<sub>17</sub>N<sub>3</sub>O<sub>5</sub>S (291.32): Calc: C, 41.23; H, 5.88; N, 14.42; S, 11.01; Found: C, 41.24; H, 5.89; N, 14.46; S, 11.03.

### Synthesis of metals complex

Cellulosic metal complexes were created by combining metal chloride (5.0 mmol) and CMSC (0.472, 2 mmol) ethanol solutions in a 2:1 ratio, followed by 6 h of heating. Items have been isolated on ice following water bath evaporation. Before drying in vacuum desiccators over anhydrous calcium chloride, all of the complexes were purified and cleaned using EtOH and diethyl ether.

C<sub>17</sub>H<sub>28</sub>CuN<sub>6</sub>O<sub>12</sub>S<sub>2</sub>: blue solid, with 77% yield, m.p.= > 300 °C, IR (KBr)  $\nu_{\max}/\text{cm}^{-1}$ :  $\bar{\nu}$  = 3323(OH), 3209 (NH<sub>2</sub>), 3044(Cu–N), 2633(C–SH), 564.5(Cu–S), 514.8(Cu–O).

C<sub>17</sub>H<sub>28</sub>CdN<sub>6</sub>O<sub>12</sub>S<sub>2</sub>: white solid, with 66% yield, m.p.= > 300°C IR (KBr)  $\nu_{\max}/\text{cm}^{-1}$ :  $\bar{\nu}$  = 3523(OH), 3321(NH<sub>2</sub>), 3155(Cd–N), 544.5(Cd–S), 529(Cd–O).

C<sub>17</sub>H<sub>28</sub>FeN<sub>6</sub>O<sub>12</sub>S<sub>2</sub>: brown solid, with 68% yield, m.p.= > 300 °C, IR (KBr)  $\nu_{\max}/\text{cm}^{-1}$ :  $\bar{\nu}$  = 3555(OH), 3213(NH<sub>2</sub>), 3123 (Fe–N), 571(Fe–S), 522(Fe–O).

Also, the fingerprint region showed absorption bands for metal oxide at 500, 600, 620 cm<sup>-1</sup> for Cd(II), Cu(II) and Fe(III), respectively, and the formation of metal oxide bond in the cellulose metal complex cannot be confirmed only by FTIR spectrum.

## Antimicrobial evaluation

### Microbial strains

The dilution method was used from 100 to 0 mg/ml as a –Ve control. Cultures of the following microorganisms were used in the tests: (i) Gram-negative bacteria: *Escherichia coli* (NCTC-10416) and *Pseudomonas aeruginosa* (NCID-9016); (ii) Gram-positive bacteria: *Staphylococcus aureus* (NCTC-7447) and *Bacillus subtilis* (NCID-3610); (iii) unicellular fungi, namely *Candida albicans* (NCCLS 11) using nutrient broth medium; (vi) filamentous fungi, namely *Aspergillus niger* (ATCC-22342) [23–25].

### Antimicrobial study

The antimicrobial studies were carried out via the turbid metric method to judge the antimicrobial activity according to the procedure described [19]. One colony of each microbial strain was suspended in a physiological saline solution (NaCl 0.9% in distilled water at pH 6.5). Mueller Hinton broth medium was inoculated by the above-mentioned bacterial strains and incubated individually at 37 °C for 24 h. After the incubation process, the turbidity was measured with a V-630 UV–Vis spectrophotometer (Jasco, Japan) at a wavelength of 530 nm, and the above concentrations were used to determine the MIC values under the same incubation conditions as observed in our previous work [11].

### Molecular docking

The Moe program was used to optimize the molecular docking of CMSC and metal complexes using bond distance [26]. As a result, the geometry optimization, a systematic conformational examination, and energy minimization of the resulting conformations using the Confirmation Examination were carried out, supported by an RMS gradient of 0.01. *Escherichia coli* MenB's crystal structure in combination with its analogous substrate, OSB-NCoA (PDB ID: 3t88) [27], the crystal structure of the tyrosine phosphatase Cps4B from *Streptococcus pneumoniae* TIGR4 (PDB ID: 2wje) [28], the crystal structure of *Aspergillus flavus* FAD glucose dehydrogenase (PDB ID: 4ynt) [29], and 1.8-angstrom refined structure of the lipase from *Geotrichum candidum* (PDB ID: 1tgh) [30]. The confirmations were determined based on the arrangement of total statistics and conformation, with the pertinent amino acids in the binding pocket for each protein, independently, using ten dispersed docking runs with default parameters.

## Analytical investigation

Metrohm model 693 VA processor and 694 VA stand equipped with three electrodes were employed. The electrodes were Ag/AgCl-3 M KCl a reference electrode and a platinum counter electrode. The carbon paste electrode CPE was used as a working electrode for electrochemical measurements and was prepared by mixing 100  $\mu$ L paraffin oil and 200 mg synthetic carbon powder 1–2 microns in an agate mortar for at least 20 min. The paste was then packed into the tip of a 1 ml insulin plastic syringe, and a copper wire was inserted to obtain the external electric contact. In the same way, several similar carbon electrodes were prepared but contained organic materials to be analyzed electrochemically, corresponding to 10% of the weights of the paste contents. Electrochemical detection was performed by cyclic voltammetry, scanning between –1.5 and 1.8 V with a rate of 100 mV/s in a 10 mL 0.05 M KCl supporting electrolyte solution. Before each measurement, the working electrode was polished and webbed with wetted tissue and the supporting electrolyte solution was purged with high-purity nitrogen gas for at least 3 min to eliminate interference from dissolved oxygen. The electronic energies of HOMO and LUMO levels were calculated by correlating the onset (starting point) of the first oxidation/reduction potentials to the vacuum energy, according to the equation  $E_{\text{HOMO/LUMO}} = -4.44 + (E_{\text{p onset}} - E_{1/2 \text{ ferrocene}}) \text{ eV}$ , where 4.44 eV is the electronic energy of the absolute standard hydrogen electrode potential relative to the vacuum energy [31, 32]. The electrode potentials of ferrocene " $E_{1/2 \text{ ferrocene}}$ " and organic materials " $E_{\text{p onset}}$ " were measured against the Ag/AgCl-3 M KCl electrode potential. On the other hand, electronic absorption spectra were measured by JASCO V-570 UV/VIS/NIR spectrometer of solutions in *N,N* Dimethylformamide DMF (spectroscopic grade). The onset of the longest wavelength absorption was used to determine the optical HOMO–LUMO gaps according to the equation  $E_{\text{g}} = 1242/\lambda_{\text{onset}}$  [12, 33].

### Computational calculations

Calculations of DFT utilized B3PW91/LANDZ2 basis set for metals utilizing the Berny method [34] were performed with the Gaussian 09W program [35, 36]. No symmetry constraints were applied during geometry optimization. Furthermore, the Gauss-View molecular visualization program was used [36]. The wide-ranging assignments of the vibrational modes were accomplished based on the potential energy distribution (PED), calculated using vibrational energy distribution analysis (VEDA) program [37, 38].



## Results and discussion

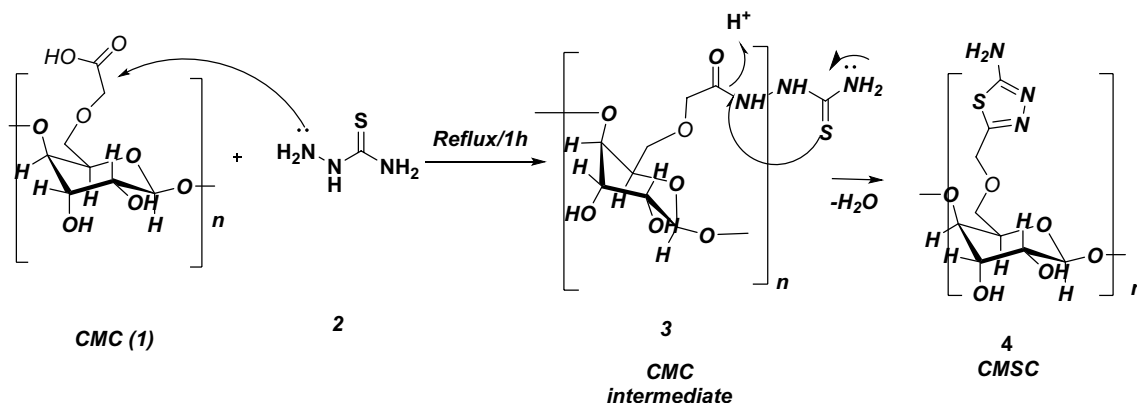
### Chemistry and metal complexes

Reactivity of carboxymethyl cellulose (CMC) (**1**) with thiosemicarbazide, (**2**) in the presence of an acidic medium undergo intermolecular cyclization to afford the corresponding (2*R*,3*R*,4*S*,5*R*,6*R*)-6-((5-amino-1,3,4-thiadiazol-2-yl)methyl)-2,5-dimethoxytetrahydro-2*H*-pyran-3,4-diol (**4**) (CMSC) as represented in Scheme 1.

The compound **4** was confirmed by spectral analysis such as FT-IR that showed characteristic bands at 3677 and 2456  $\text{cm}^{-1}$  for OH and  $\text{NH}_2$ , respectively. Consequently, some observations were noticed including that through delocalization of a unique couple of electrons on nitrogen to and afford the corresponding monomer of 2-(2-((2*R*,3*R*,4*S*,5*R*,6*R*)-4,5-dihydroxy-3,6-dimethoxytetrahydro-2*H*-pyran-2-yl)acetyl) hydrazine-1-carbothioamide intermediate (**3**) which showed the conjugation and delocalization result and attack of  $\text{C}=\text{S}$  to  $\text{C}=\text{N}$  to afford the monomer of

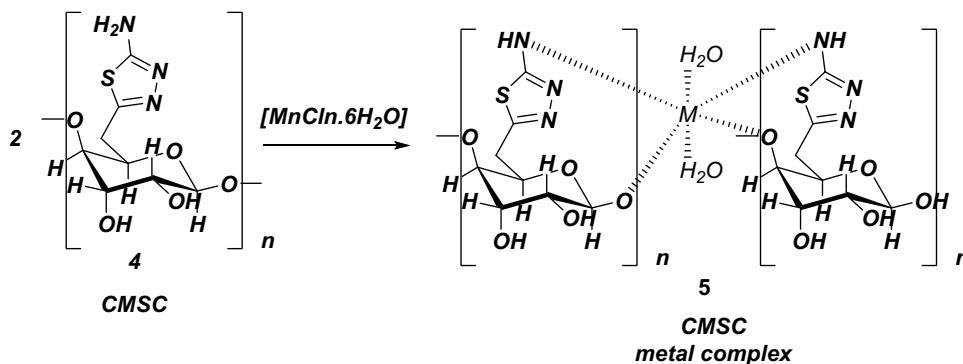
(2*R*,3*R*,4*S*,5*R*,6*R*)-6-((5-amino-1,3,4-thiadiazol-2-yl)methyl)-2,5-dimethoxytetrahydro-2*H*-pyran-3,4-diol (**4**) (CMSC). The attack of the amino group of thiosemicarbazide of  $\text{C}=\text{O}$  of  $\text{COOH}$  of CMC and then cleavage of the water molecule to give the corresponding 5-amino-1,3,4-thiadiazol cellulose moiety (CMSC) and the  $^1\text{H}$ NMR of this compound showed the formation of the amino signal at 6.39 ppm and more aliphatic region from 2.40 to 5.08 ppm due to cellulose ring as displayed in Scheme 1.

The reactivity of 5-amino-1,3,4-thiadiazol cellulose toward metal chlorides  $\text{Cu(II)}$ ,  $\text{Cd(II)}$ , and  $\text{Fe(III)}$  was obtained via ligand/metal ratio (2:1); the ligand and its metal complexes were stable at 27 °C and are mostly soluble in DMF and DMSO [39]. As shown in Scheme 2, we noticed that the amino group in 5-amino-1,3,4-thiadiazol cellulose was chelated with metals through a hydrogen bond. The obtained complexes with high melting points and investigated through TGA and also were investigated through FT-IR which were noticed that the presence of  $\text{NH}_2$  in CMSC at  $\bar{\nu} = 3300 \text{ cm}^{-1}$  which decreased in metal complexes to 3209, 3321, and 3213 for  $\text{Cu(II)}$ ,  $\text{Cd(II)}$  and  $\text{Fe(III)}$  [40], respectively.



**Scheme 1** Reaction of carboxymethyl cellulose with thiosemicarbazide

**Scheme 2** Complexation of 5-amino-1,3,4-thiadiazol cellulose with metal chlorides



## Characterization of CMC, CMSC, and metal complexes

### FT-IR investigation

Figure 2A shows the structural characterization of CMC and CMSC. The typical peaks of stretching vibration -OH groups appear at  $3500\text{ cm}^{-1}$  in the pure CMC spectrum, which is a useful tool for FT-IR analysis in elucidating chemical structure and bond formation, and stretching at  $2900\text{ cm}^{-1}$ , C–O–C ether linkage at  $1180\text{ cm}^{-1}$ , and CH stretching at  $2900\text{ cm}^{-1}$ . Due to the carboxyl group ( $\text{C}=\text{O}$ ), the peak was visible at  $1700\text{ cm}^{-1}$ . A new absorption band with a double beak develops in the spectra of CMSC, indicating the presence of an  $\text{NH}_2$  peak in this area for CMSC with intramolecular OH groups of CMC. In addition, it was found that N–H bending vibration existed at  $1500\text{ cm}^{-1}$ . Moreover, the CMSC fingerprint region contains distinct distinctive absorption bands at  $1400\text{ cm}^{-1}$  due to CH aliphatic and  $1020\text{ cm}^{-1}$  at C–N of the amino group, respectively. The presence of  $\text{NH}_2$  for CMSC was noted at a range of  $3300\text{ cm}^{-1}$ , and it was noted that the metal complexes Cd(II), Cu(II), and Fe(III) are shielded in this peak at  $3400\text{--}3500\text{ cm}^{-1}$  due to the formation of a coordination bond between the metal and  $\text{NH}_2$  and be NH group, in addition to the presence of stretching -OH groups of cellulose. Moreover, the presence of strong absorption bands between  $1660$  and  $1600\text{ cm}^{-1}$  caused by the thiazole ring's C=C bending alkene [41], The C–N absorption band is at  $1400\text{ cm}^{-1}$ , the C–O–C stretch is at  $1250\text{ cm}^{-1}$ , and the C–OH stretch is

at  $1200\text{ cm}^{-1}$ , where all metals and CMSC are complex. Additionally, the fingerprint region displayed metal oxide absorption bands at  $529$ ,  $514.8$ , and  $522\text{ cm}^{-1}$  for Cd(II), Cu(II), and Fe(III), respectively, as well as the Cu–S( $564.4$ ), Cd–S( $544.5$ ), and Fe–S( $571$ ), as shown in Fig. 2B. Additionally, there are bending vibrations of the cellulose backbone in region  $900\text{--}400\text{ cm}^{-1}$ .

### XRD of cellulosic complexes

The breakdown of the CMC chain caused by the creation of the metal complex is seen in Fig. 3 and is used to characterize the crystallinity of the CMC and metals complex. CMC displayed two diffraction peaks at  $2\theta$  of  $10$  and  $20^\circ$  due to amorphous and crystalline regions, respectively. These peaks disappeared due to metals chelation and new peaks appeared at  $2\theta = 35, 45$  for Cd,  $2\theta = 35$  for Fe, and  $2\theta = 40, 45$  for Cu which means that metals complexes and the chelation have destroyed the CMC morphology structure (microcrystalline and amorphous) [13, 42]. The Cd–O showed at  $2\theta = 45$ , while the Cu–O and Fe–O showed at  $2\theta = 40$  shown in Fig. 3A–C.

### Thermal analysis (TGA)

Figure 4 displays the thermogravimetric analysis of CMC and metals complex composite. The thermal stability behavior of CMC has occurred via three steps; the first was up to  $100^\circ\text{C}$  due to humidity removal with weight loss of about 5%. In the second step, successive degradation occurred at

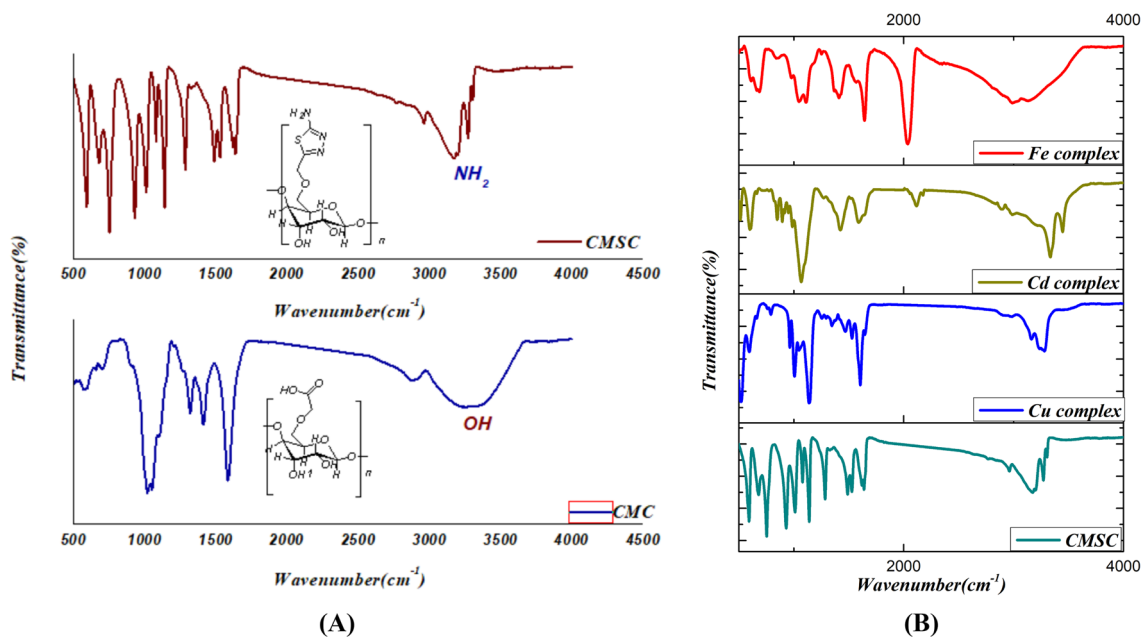


**Fig. 2** **A** FT-IR of CMC and CMSC, **B** FT-IR spectrum of CMSC metal complexes

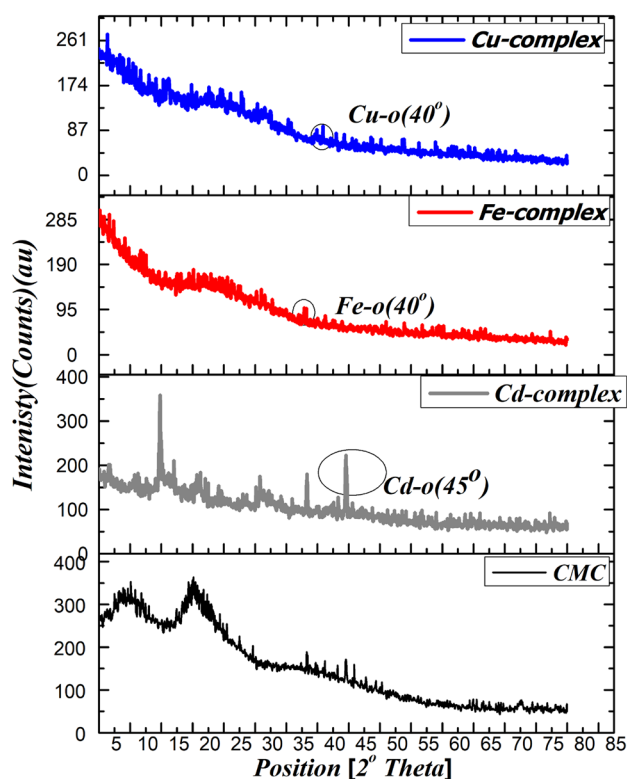


**Fig. 3** XRD of CMC, CMSC metal complexes

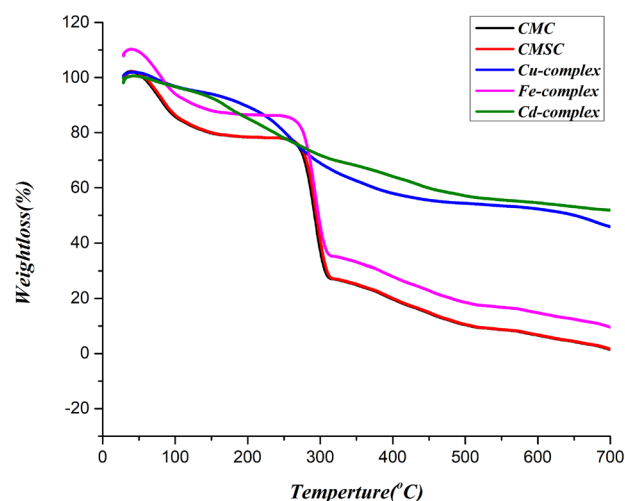


**Fig. 4** TGA of CMC, CMSC, and CMSC metal complexes

temperatures 200–300 °C with weight loss of about 80%. Finally, the most weight degradation occurred above 300 °C with a residue of about 10%. The CMSC showed stability behavior at 300 °C, and the metal chelation of CMSC with Cu(II), Fe(III), and Cd(II), respectively, showed thermal stability higher than pure CMSC. The metal complex composite was characterized by thermal instability in the early

stage due to humidity removal at 100 °C; this stage was followed by thermal degradation with weight loss of about 32%, 40%, and 45% for Cd(II), Cu(II) and Fe(III) due to formation of metal oxide, respectively, at a temperature above 300 °C.

## Scanning electron microscope (SEM)

The surface morphology of CMC, CMSC, and metal complexes was investigated through an SEM with a high magnification of 140kX. All investigated cellulosic derivatives CMC and complexes matrixes were homogenous sponge surfaces. As seen in Fig. 3, it was noticed that the fibers of CMC with tied bundles on each other with no pore sizes this bundle has destroyed as it seems in the CMSC image. A highly rough surface appears on the surface of CMSC as small needles due to the formation of amino cellulose on the CMC surface. Furthermore, the CMSC had multi-coordination sites like NH<sub>2</sub> and OH groups through its efficiency through metal complexes; the Cd(II) showed a white foam surface (smooth surface) with pores with different diameters between 5–20 nm with un-separated vacancies' between pores, while Cu(II) complex showed as white cracks with needles on the surface with needle diameter size ranging between 100 nm, also Fe(III) complex showed that ice rough solid surface on cellulose surface with size ranging between 250 nm. So we concluded that the metal chelate on the surface of cellulose changes the surface of homogenous and bundle structure of CMC and CMSC which confirms the chelation of all surfaces of cellulose and coating it from all sides as shown in Fig. 5.

## Biological evaluation

### Antimicrobial activities

Antimicrobial activity has a significant role in biological activity. Indeed, the insoluble material antimicrobial activity detection is very stable to determine via the turbidimetric method [43]. Anywhere the turbidimetric technique was performed as the simulated method for the solid material in general applications. The eukaryotic and prokaryotic microbial cells are presented in this study. The ligand material has slightly antimicrobial activity. Additionally, the addition of metals enhances the sample's antimicrobial activity. In general, Cu shows excellent antimicrobial activity followed then Cd and Fe (Fig. 6). Where, MICs values of tested metals complex observed low values for all tested metals samples against gram-positive, gram-negative, and fungi strains. Cd and Fe complexes observed the appropriate values of MICs where the concentration of about 6.25 µg/ml is adequate to inhibit all microbial populations. On the other hand, the

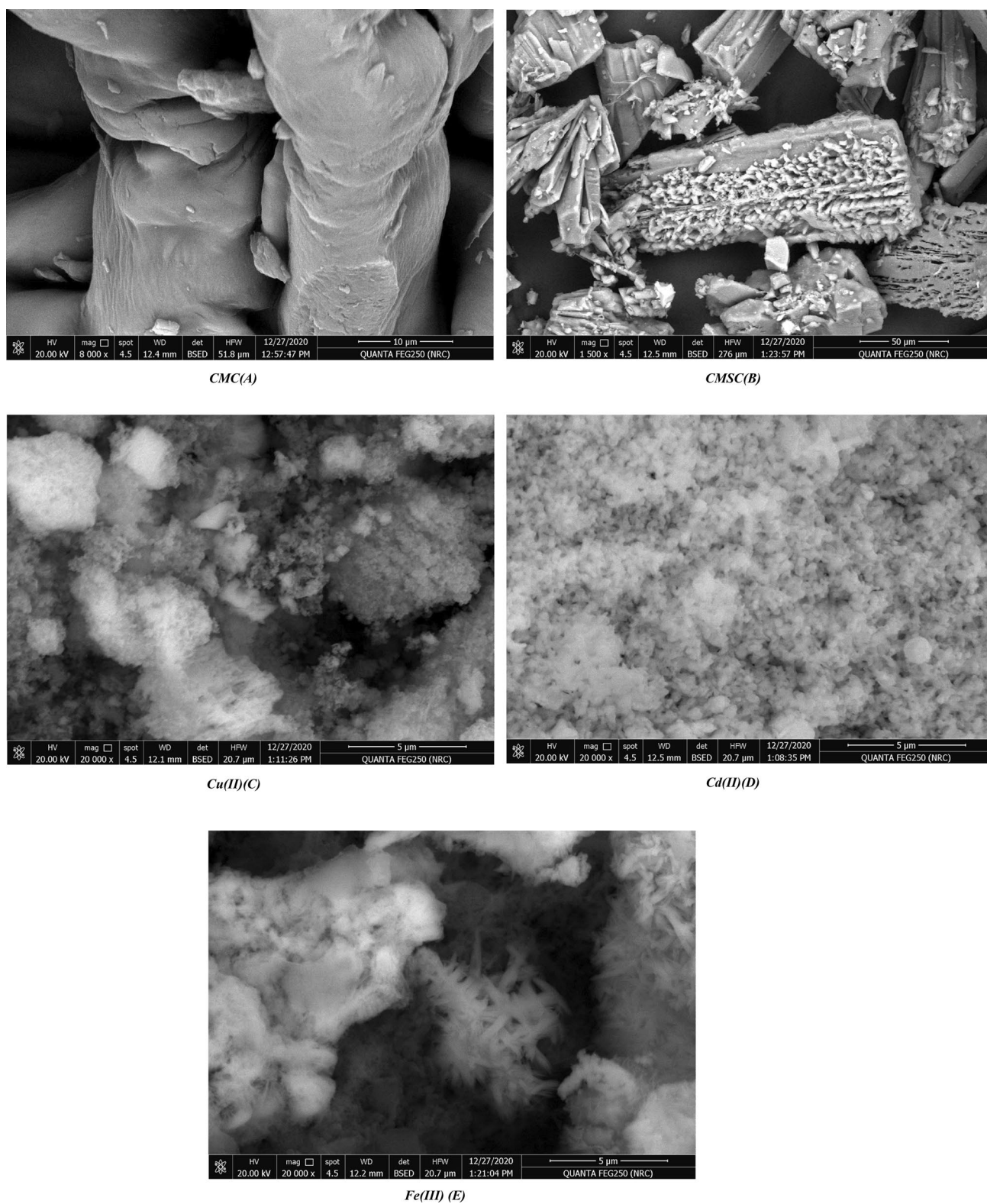
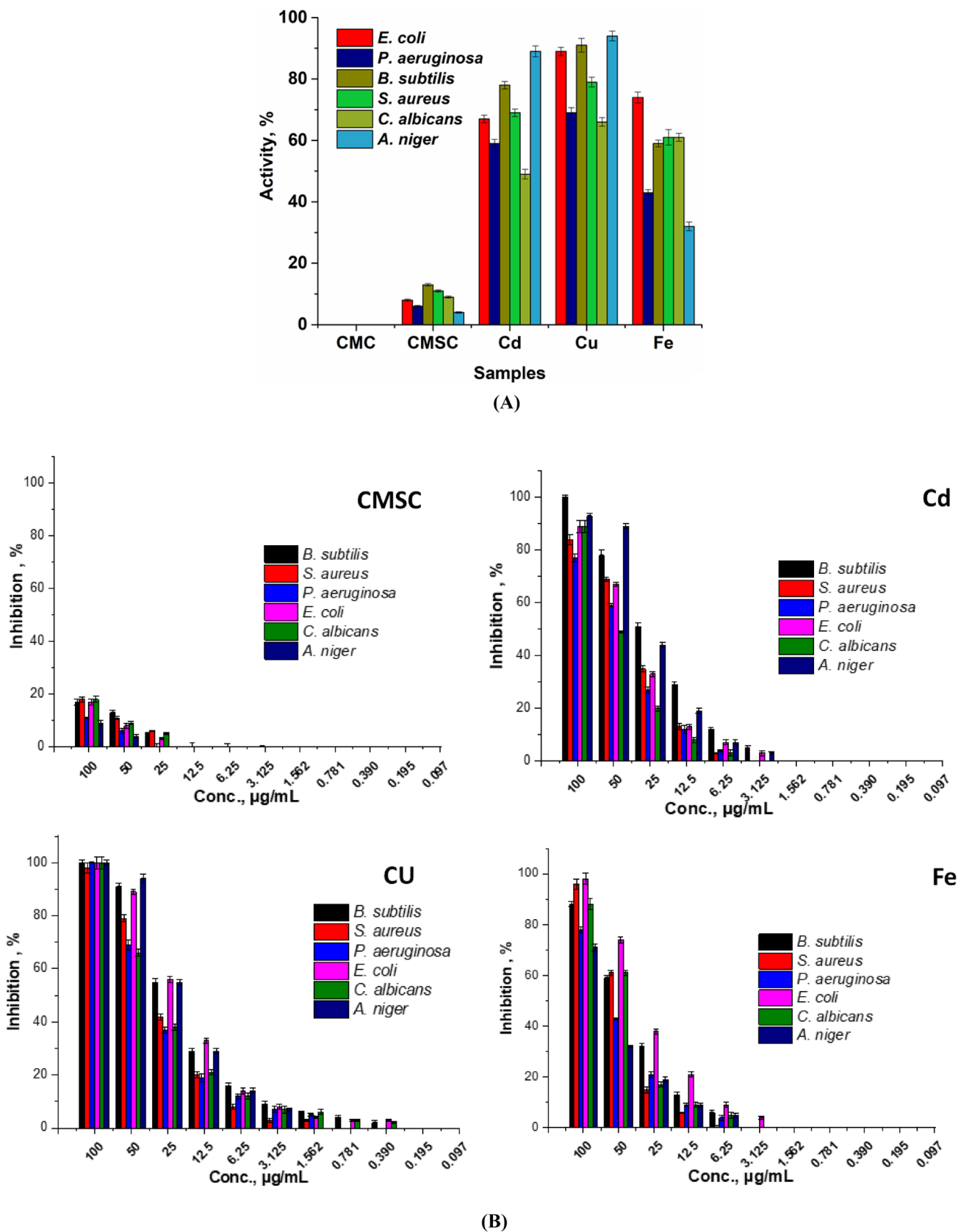


Fig. 5 SEM of CMC, CMSC, and CMSC metal complexes



**Fig. 6** Antimicrobial activity percentage for cellulosic metal complexes (50 µg/ml) against tested organisms (A) and MICs of the tested samples against tested microorganisms (B)



Cu complex performed an excellent MICs value where the MIC value in which all microbial populations are inhibited is 1.562 µg/ml. Moreover, the concentration of 0.39 is effective to inhibit gram-negative bacteria. Overall nanomaterials are deformed to cellular enzymes and DNA by coordinating with electron-donating groups and destroying the cell membrane's selective permeability [44, 45]. However, some metals are used as micronutrients by microorganism, e.g., iron and cadmium which are involved in many metabolic pathways and enzyme structure this explain the superiority of copper [46]. The above finding affirmed that the characterization of the prepared samples were solve the understating of the antimicrobial activity for each one. The CMC lacked any antimicrobial activity whereas is a polymer of glucose with a carboxy group which has not any antimicrobial activity. Otherwise, the CMCS contains amine group which play a role in antimicrobial activity [45]. Additionally, the metal complexes observed excellent antimicrobial activity as a result of the synergetic effect of amino group activity and the role of metals to deactivate microbial activity via different mechanisms [47–49].

## Docking stimulation

CMSC and metals complex docking research for the Moe program [50] to identify and characterize the biological activity of different amino groups of CMSC and metals which were found to be compatible with the experimental results. Docking of these compounds against the crystal structure of *Escherichia Coli MenB* in complex with substrate analog, OSB-NCoA (PDBID:3t88) [27], showed the most stable compound CMSC with  $-10.4680$  kcal/mol and with short bond distance 3.02 Å, 1.45 Å, 2.62 Å with different proteins (Arg 230, Gli 248, Arg 64, Tyr 65); this is because the presence of NH<sub>2</sub> bounded to cellulose moiety led to the presence of several amino groups which increase its in-silico studies. The metal complexes Cu(II), Fe(III), and Cd(II) showed high binding energy with  $-10.5659$  kcal/mol,  $-11.6577$  kcal/mol, and  $-11.0558$  kcal/mol, respectively, with a bond length range of 1.5–3.25 Å and different types of proteins due to the presence of NH<sub>2</sub> group which attached to glycoside nucleus with several proteins (Tyr 170, Asn 202, Arg 173, Asp 142), (Asp 239, Arg 173, Ile 174, Leu 236) and (Asn 202, Leu 143, Leu 236) due to the metal chelation and more adsorption on the surface of cellulose and make more attachments with different proteins.

Similarly, the Crystal structure of the tyrosine phosphatase Cps4B from *Streptococcus pneumoniae* TIGR4 (PDBID:2wje) [28] attached with CMSC and metal complexes with  $-11.7051$ ,  $-12.1088$ ,  $-11.9250$ , and  $-12.7961$  kcal/mol and a least bond distance 1.75 Å, 3.43 Å with (Lys 45, Tyr 82, Thr 84), (Gly 205, Lys 171, Ser 165,

Arg 176), (Lys 171, Tyr 177, Gly 205, Arg 176) and (Lys 171, Gly 205, Tyr 177), respectively.

Designation of the Crystal structure of *Aspergillus flavus* FAD glucose dehydrogenase (PDBID:4ynt) [29] with the CMSC and metals complex confirmed that the most stable compound is CMSC with proteins (Val 369, Asn 424, Asn 298, Ser 428) at binding energy  $-11.1898$  kcal/mol and distance 2.97 Å, 1.58 Å, 1.68 Å, 2.98 Å mostly attached to C=O group, also the Cd complex showed  $-10.6527$  kcal/mol (Asp 251, Lys 241, His 266, Asn 242) with attached bond length 1.32 Å, 1.86 Å where these proteins attached to thiazole ring. Also, the reactivity of Fe complex is  $-8.4781$  kcal/mol with binding energy for protein (Tyr 199, Ser 33, Asn 51, Gly 94) with bond length (1.42 Å, 2.58 Å) due to the amino of thiazole and OH groups of cellulose as shown in Fig. 7. Furthermore, the investigation of these triazole rings with 1.8 Å refined structure of the lipase from *Geotrichum candidum* (PDB ID: 1tgh) [30] is displayed in Fig. 7. The Fe complex compound showed least binding energy rather than other compounds with  $-11.5321$  kcal/mol which attached to Gly 195, His 188, Tyr 230, His 41 with 2.85 Å, 2.81 Å, 2.64 Å to NH<sub>2</sub> groups, Cu complex, and Cd complex class showed good stability in protein pocket with binding energy  $-10.0548$ , and  $-11.2576$  kcal/mol which attached with less bond distance range 1.37–2.83 Å and give the stability of these metals inside the pocket [51] (Table 1).

## Electrochemical analysis

### Cyclic voltammetry

In the potential range of interest (between  $-1.5$  and  $1.8$  V), no electroactive activities are observed in the absence of organic materials. In the presence of ferrocene, reversible ferrocene/ferrocenium Fc/Fc<sup>+</sup> redox process is exhibited as an internal standard in 0.05 M KCl and its half potential  $E_{1/2}$  is measured to be 0.431 V against Ag/AgCl, 3 M KCl. Electrochemical characterization of four organic moieties at the carbon paste interface exhibited irreversible oxidation and quasi-reversible oxidation/reduction processes as displayed in Fig. 8A. The first one reveals two overlapped irreversible oxidation peaks arising probably from the electrochemical C–C bond cleavage of vicinal diol in cellulosic derivatives, CMC and CMSC, form in sequential aldehyde at about 0.35 V and then the carboxylic group at about 0.85 V. This conclusion supports through a research article demonstrated that two oxidation peak potentials were detected at ca. 0.09 V and ca. 0.24 V on gold electrode under the alkaline conditions and could be applied successfully as a direct electrical-based fuel source. Furthermore, the LUMO levels of CMC ( $-1.2$  eV)

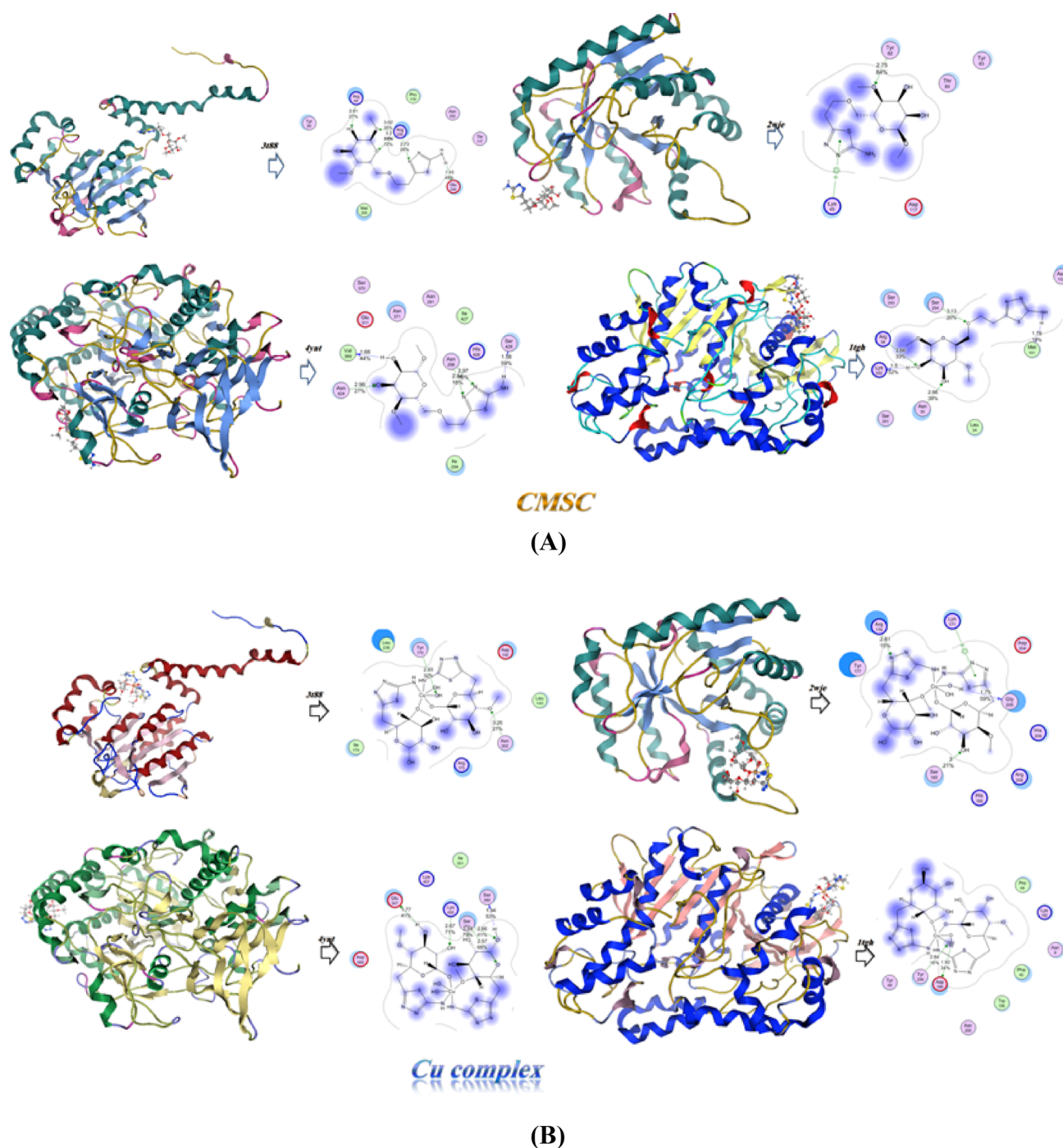


**Fig. 7** Modes of docking cellulosic and metal complexes with different proteins

and CMSC ( $-2.2$  eV) are lower than the conduction band of a semiconductor such as  $\text{TiO}_2$  ( $-3.2$  eV) and nominated to act as an electrolyte in the fabrication of organic fuel cells. But on binding CMSC with different divalent metal ions, a massive drop in energy levels LUMO is shown in the order  $\text{Cd} > \text{Cu} > \text{Fe}$  as demonstrated in Table 2 and Fig. 8A. This attributes to binding strengths between metal

and CMSC which decrease in the molar absorptivity, i.e., hypochromic effect, and increase to longer wavelengths, i.e., bathochromic shift as displayed in Fig. 8B. On applying the cyclic voltammetry, the metals complex undergoes two electrochemical processes, one due to the irreversible oxidation of CMSC and another due to the quasi-reversible reaction of metals. As shown in Fig. 8C, Cu(II)

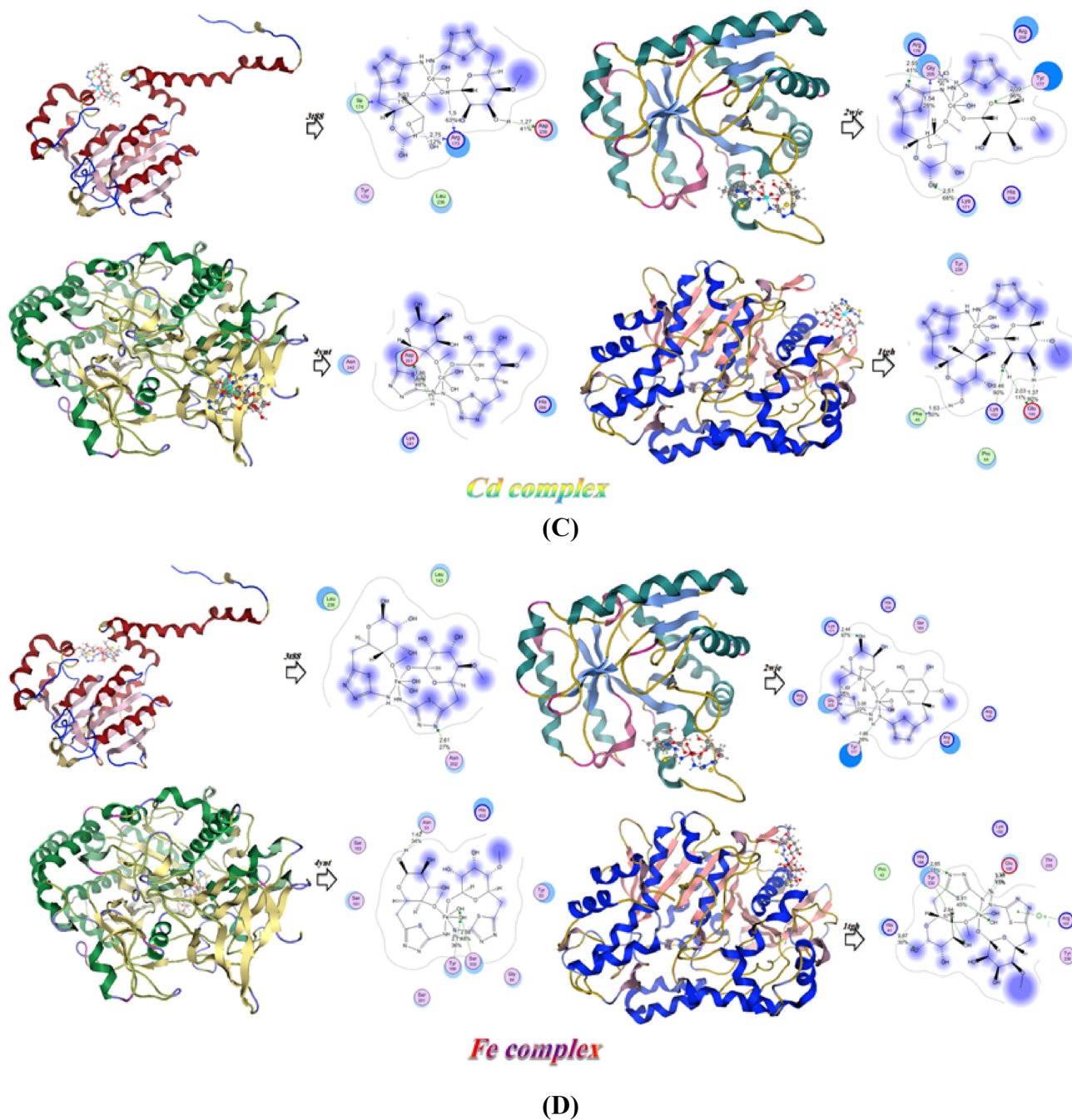


Fig. 7 (continued)

complex displays the characteristic of the electric double-layer capacitance enhancing the electrochemical activity of the redox materials at the interface.

The LUMOs values given in the 3rd column were estimated by the cyclic voltammetry, while given in the 7th column were estimated by the UV–Vis spectrophotometry.

Based on each spectrum, the optical energy gap  $E_g$  can be estimated according to the following equation [1].

$$E_g = h \times f = h \times \frac{c}{\lambda_{eg}} \sim \frac{1242}{\lambda_{eg}} \quad (1)$$

$E_g$  represents the optical band gap expressed in eV and  $\lambda_{eg}$  denotes the absorption edge wavelength expressed in nm, obtained from the offset wavelength derived from the low energy absorption band as schematically represented in Fig. 9.

**Table 1** Molecular docking pose of CMSC and metals complex with different proteins

<i>Escherichia coli</i> (PDB:3t88)			<i>Streptococcus pneumoniae</i> (PDB:2wje)				
	Energy affinity (kcal/mol)	Distance(Å)	Amino acids		Energy affinity (kcal/mol)	Distance(Å)	Amino acids
CMSC	−10.4680	3.02 Å, 1.45 Å, 2.62 Å	Arg 230, Gli 248, Arg 64, Tyr 65	CMSC	−11.7051	2.75 Å	Lys 45, Tyr 82, Thr 84
Cu-chelate	−10.5659	2.93 Å, 3.25 Å	Tyr 170, Asn 202, Arg 173, Asp 142	Cu-chelate	−12.1088	1.75 Å, 3 Å, 2.81 Å	Gly 205, Lys 171, Ser 165, Arg 176
Cd-chelate	−11.6577	1.5 Å, 1.27 Å, 2.75 Å	Asp 239, Arg 173, Ile 174, Leu 236	Cd-chelate	−11.9250	2.55 Å, 3.43 Å, 2.51 Å	Lys 171, Tyr 177, Gly 205, Arg 176
Fe-chelate	−11.0558	2.61 Å	Asn 202, Leu 143, Leu 236	Fe--chelate	−12.7961	1.85 Å, 1.49 Å, 2.44 Å	Lys 171, Gly 205, Tyr 177
<i>Aspergillus flavus</i> (PDB:4ynt)			<i>Geotrichum candidum</i> (PDB:1tgh)				
	Energy affinity (kcal/mol)	Distance(Å)	Amino acids		Energy affinity (kcal/mol)	Distance(Å)	Amino acids
CMSC	−11.1898	2.97 Å, 1.58 Å, 1.68 Å, 2.98 Å	Val 369, Asn 424, Asn 298, Ser 428	CMSC	−9.3416	1.78 Å, 3.13 Å, 2.66 Å, 1.5 Å	Lys 292, Arg 36, Asn 35, Ser 294
Cu-chelate	−7.2651	1.94 Å, 2.66 Å	Lys 450, Ser 251, Ser 350, Gly 347	Cu-chelate	−10.0548	1.92 Å, 2.84 Å	Tyr 236, Asp 199, Tyr 49
Cd-chelate	−10.6527	1.32 Å, 1.86 Å	Asp 251, Lys 241, His 266, Asn 242	Cd-chelate	−11.2576	1.37 Å, 1.63 Å, 2.03 Å	Lys 192, Glu 195, Phe 45, Pro44
Fe-chelate	−8.4781	1.42 Å, 2.58 Å	Tyr 199, Ser 33, Asn 51, Gly 94	Fe-chelate	−11.5321	2.85 Å, 2.81 Å, 2.64 Å	Gly 195, His 188, Tyr 230, His 41

## Computational calculations

The optimization of the one unit of cellulose m(CMC), thiosemicarbazide, m(CMSC) utilizing DFT/ B3PW91/LANDZ2 basis set with Gaussian 09 [53] and showing their physical properties for example absolute electronegativities ( $\chi$ ), chemical potentials ( $\mu$ ), absolute hardness ( $\eta$ ), absolute softness ( $\sigma$ ), global electrophilicity ( $\omega$ ), global softness ( $S$ ), and additional electronic charge, ( $\Delta N_{\max}$ ) is scheduled in Table 3 and Fig. 10 according to the following equations [4, 14, 18, 54]. These CMC, thiosemicarbazide, CMSC, and metal complexes were not plane and takes different angles

$$\Delta E = E_{\text{LUMO}} - E_{\text{HOMO}} \quad (2)$$

$$\chi = \frac{-(E_{\text{HOMO}} + E_{\text{LUMO}})}{2} \quad (3)$$

$$\eta = \frac{(E_{\text{LUMO}} - E_{\text{HOMO}})}{2} \quad (4)$$

$$\sigma = 1/\eta \quad (5)$$

$$\mu = -\chi \quad (6)$$

$$S = 1/2\eta \quad (7)$$

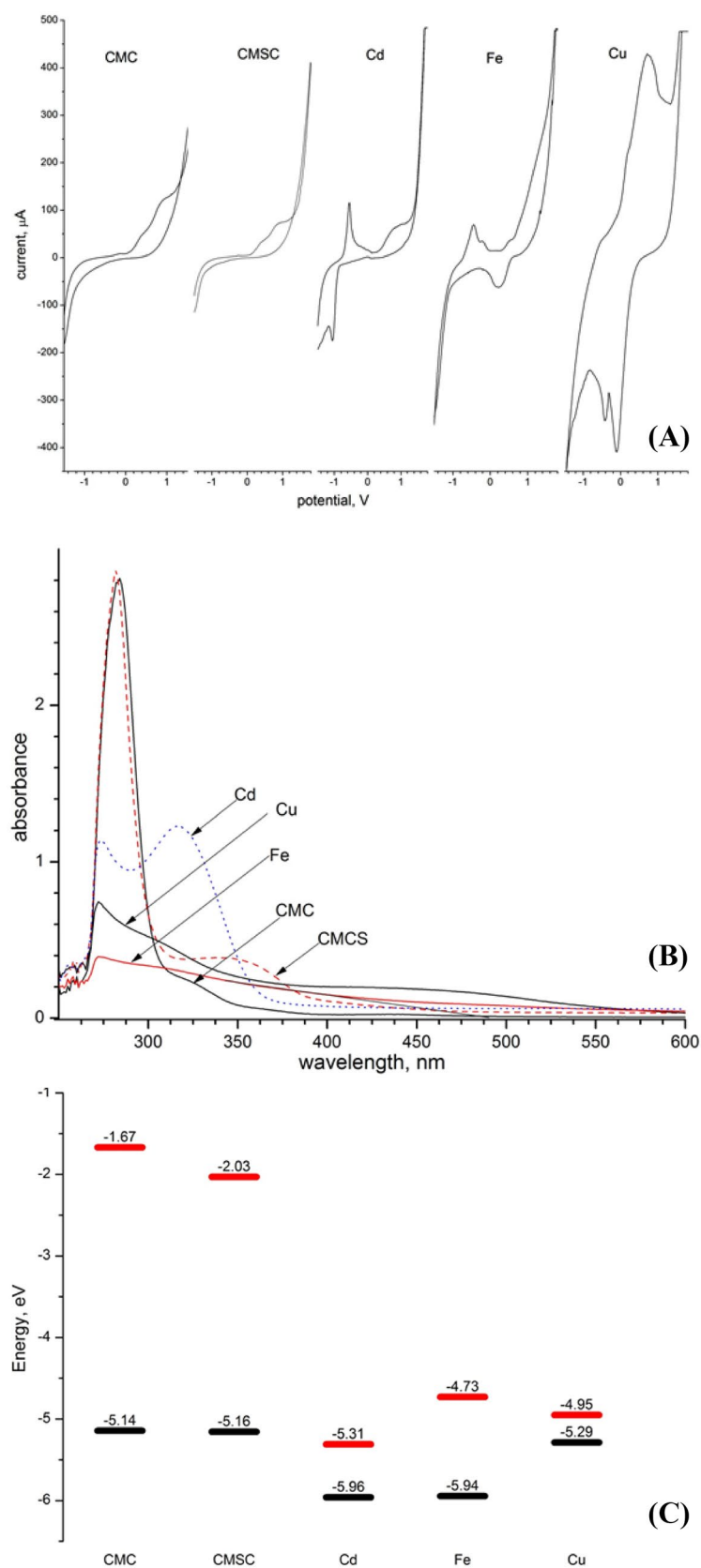
$$\omega = \mu^2/2\eta \quad (8)$$

$$\Delta N_{\max} = -\mu/\eta \quad (9)$$

From DFT/ B3PW91/LANDZ2 and their physical parameters, we noticed that there is possible interaction of this reaction which is clarified as the HOMO–LUMO interaction of CMC with thiosemicarbazide as HOMO–LUMO<sub>1</sub> as ( $\Delta E = 6.316\text{eV}$ ) with HOMO–LUMO<sub>2</sub> of thiosemicarbazide was ( $\Delta E = 5.4656\text{eV}$ ) as presented in Fig. 4 to afford the thiosemicarbazide intermediate with ( $\Delta E = 0.389395\text{eV}$ ) which is cyclized to afford them(CMSC) with ( $\Delta E = 5.700516\text{eV}$ ) which gave its stability and more reactivity and amino group make more electron distribution for can easily react again. Additionally, the chemical hardness  $\eta$  (eV) indicates the extent resistance of change of electron cloud density in the system; we noticed that CMSC has a low value compared with CMC through ( $0.308\text{eV}$ ) ( $\approx 7.10265\text{ kcal/mol}$ ), and thiosemicarbazide with ( $24.47\text{ eV}$ ) ( $\approx 564.291\text{ kcal/mol}$ ) which gave it the ability for cyclized easy and gave CMSC Molecular electrostatic potential (ESP) that the atom of a molecule generates the surrounding space which



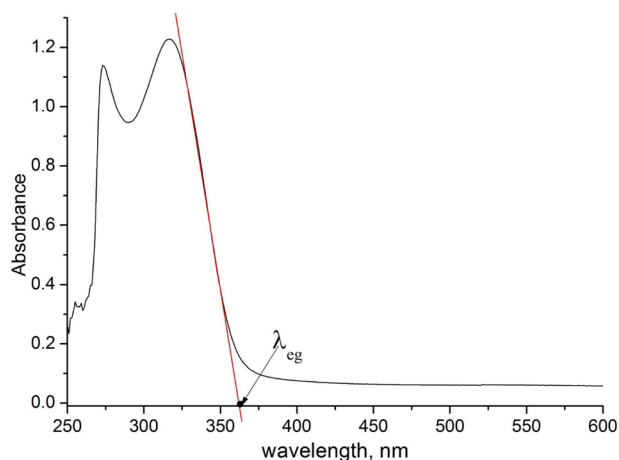
**Fig. 8** Cyclic voltammetry of cellulosic and metal complexes with a sweep rate of 100 mV/s in aqueous 0.05 M KCl solution (A), UV Absorption spectrum, and optical band gap (B) and Energy Band Diagram (C)





**Table 2** Electronic properties of CMC, CMSC, and metal complexes

Compound	Reduction potential $E_c$ onset (V)	LUMO (eV)	Oxidation potential $E_a$ onset (V)	HOMO (eV)	Optical energy gap $E_g$ (wV)	LUMO (eV)
CMC	–	–	0.137	–5.144	3.476	–1.668
CMSC	–	–	0.125	–5.156	3.125	–2.031
Cd	–0.029	–5.31	–0.678	–5.959	3.431	
Fe	0.55	–4.731	–0.663	–5.944	2.542	
Cu	0.329	–4.952	–0.006	–5.287	2.202	

**Fig. 9** Shows, as an example, the treatment of the UV–Vis spectrum of the Cd complex, to show in detail how the onset wavelength is determined, which eventually leads to the calculations of the  $E_g$  value [52]

is important to elucidate the molecular action, and biological recognition interactions. So, the **CMSC** designate a certain point which indicates that there is a uniform distribution of surface contour for these rings rather than the other compound because they have contains the C=N, C=S, and O atom which act as electrophilic centers which induced more protonation and gave more reactivity in the biological interaction and the binding sites of proteins in molecular docking [36, 43, 55] as demonstrated in Fig. 10.

### Optimization of metal complexes

The optimization of metal cellulose complexes Cu(II), Cd(II), and Fe(III) were elucidated utilized DFT/B3PW91/LANDZ2 basis set are used to demonstrate the environment and stability of these complexes. Calculated geometrical parameters are bond angles, bond lengths, and dihedral angles, natural charges on active centers, and the energetic

**Table 3** Physical analysis of compounds CMC, thiosemicarbazide, and CMSC utilizing DFT/ B3PW91/LANDZ2

	DFT/B3PW91/LANDZ2							
	m(CMC)	Thiosemicarbazide	Intermediate m(CMSC)	m(CMSC)				
$E_T$ (au)	–878.839	–603.428	–1405.70965	–1483.2279				
$E_{HOMO}$ (au)	–0.24630	–0.18346	–0.25861	–0.21588				
$E_{LUMO}$ (au)	–0.01416	0.01740	–0.2443	–0.00639				
$E_g$ (eV)	6.3168	5.4656	0.389395	5.700516				
$\mu$ (D)	2.1691	7.0010	4.5431	5.6515				
$\chi$ (eV)	7.087481	4.5187249	6.84244234	3.02413883				
$\eta$ (eV)	3.1584271	27.32841	0.19469756	2.85025799				
$\sigma$ (eV)	234.439536	27.0948798	5.136171198	0.3508454				
$P_i$ (eV)	–7.08748098	–4.51872492	–6.84244234	–3.02413883				
$S$ (eV)	1.57921354	13.663388	0.09734878	0.175422716				
$\omega$ (eV)	0.1069408	0.37660576	4.55777420	13.032217				
$\Delta N_{max}$	61.062107	4.4991327	35.14395527	1.05964912				
Net charges								
	C <sub>17</sub>	0.494	N <sub>1</sub>	–0.562	N <sub>24</sub>	–0.365	N <sub>24</sub>	–0.753
	O <sub>20</sub>	–0.556	N <sub>2</sub>	–0.442	N <sub>21</sub>	–0.543	N <sub>21</sub>	–0.287
	H <sub>21</sub>	0.386	N <sub>5</sub>	–0.722	N <sub>20</sub>	–0.643	N <sub>20</sub>	–0.223
	O <sub>19</sub>	–0.421	C <sub>3</sub>	0.227	C <sub>22</sub>	0.1232	C <sub>22</sub>	0.134
	C <sub>13</sub>	–0.299	S <sub>4</sub>	–0.192	S <sub>23</sub>	–0.184	S <sub>23</sub>	0.490
	O <sub>1</sub>	–0.527	H <sub>6</sub>	0.338	H <sub>36</sub>	0.273	H <sub>36</sub>	0.340

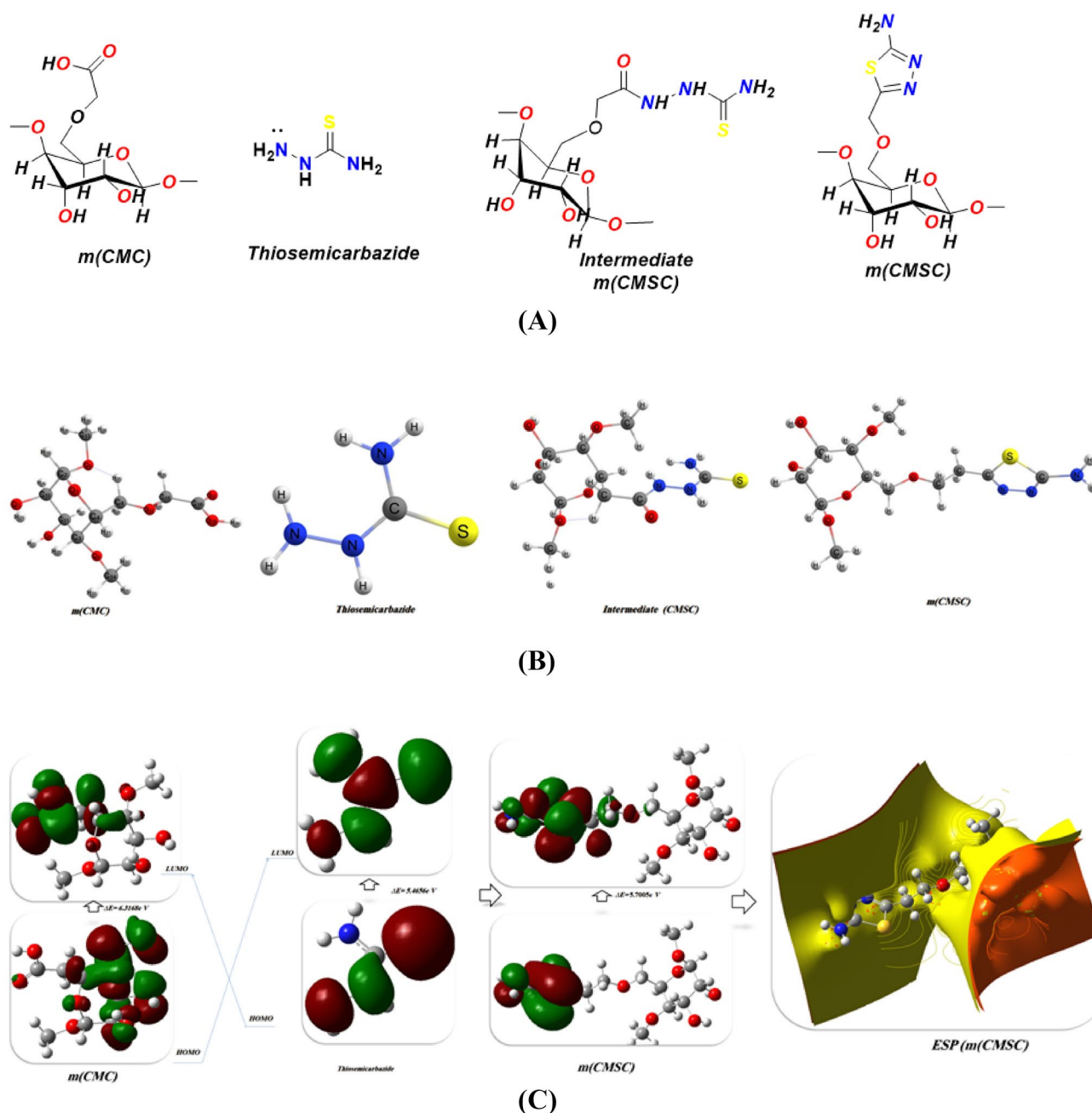


**Fig. 10** Chemical and optimized structure, compounds *m*(CMC), thiosemicarbazide, intermediate *m*(CMSC), and *m*(CMSC) using DFT/B3PW91/LANDZ2 (A, B) FMO and ESP of *m*(CMC), thiosemicarbazide and *m*(CMSC) and (C)

of the optimized ground state for the studied chelates. These geometrical parameters together with the practical spectroscopic data proved that the metal ions are coordinated to the ligand via (N, O, and S) atoms forming stable chelates. These results indicate that; in Cu(II), Cd(II), and Fe(III) metal complexes, the metal ion coordinates with N<sub>68</sub> and N<sub>34</sub> with O<sub>71</sub>, O<sub>72</sub> and mask the cellulose from these two sites which refer that regular distorted octahedral geometry for all the metal chelates. Also, we noticed that the three

complexes were near to each other's in the energy with range (−2152.5433 to −2155 au) with ligand: metal ration 2:1, as shown in Fig. 11 it was metal complexes were no in the same planar and also their dipole moment similar to each other's which all have easily charge separation and gave it more reactivity [56–59].

Global reactivity descriptors of CMSC, Cu(II), Cd(II), and Fe(III) chelates using the DFT/B3PW91/LANDZ2 basis set we noticed the difference in energy between the

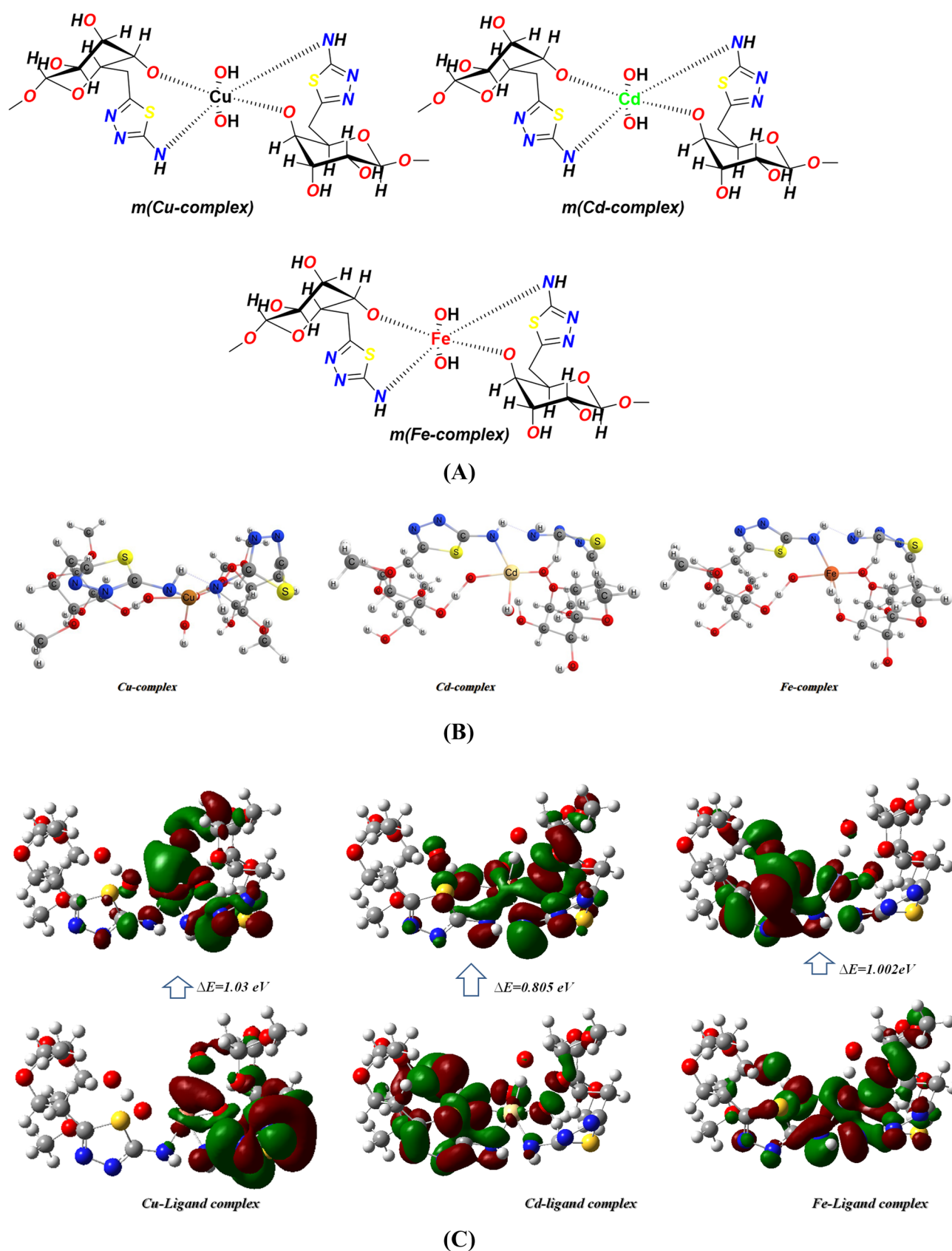


**Fig. 11** **A, B** The chemical structure and optimized structures of metal complexes; **C** FMO of metal complex utilized DFT/ B3PW91/LANDZ2 basis set

**Table 4** Physical descriptors of CMSC, Cu(II), Cd(II), and Fe(III) chelates utilized DFT/B3PW91/LANDZ2 basis set

	DFT/ B3PW91/LANDZ2(d)					
	Cu(II)	Cd(II)	Fe(III)			
$E_T$ (au)	-2152.5433	-2154.6303	-2155.020			
$E_{HOMO}$ (au)	-0.23452	-0.21116	-0.22624			
$E_{LUMO}$ (au)	-0.18654	-0.18141	-0.18915			
$E_g$ (eV)	1.3056029	0.8095	1.0092			
$\mu$ (D)	7.0502	7.4054	7.1043			
$\chi$ (eV)	5.7288158	5.34118945	5.65167152			
$\eta$ (eV)	0.65280146	0.40476956	0.018545			
$\sigma$ (eV)	1.5318593190	67.2268907	53.9228902669			
$P_i$ (eV)	-5.7288158	-5.34118945	-5.65167152			
$S$ (eV)	0.32640073	0.20238478	0.0092725			
$\omega$ (eV)	10.71225342	5.7736946787	0.2961765477			
$\Delta N_{max}$	8.7757398704347	13.1956302494	302.830951739			
Net charges	Cu <sub>74</sub>	0.456	Cd <sub>75</sub>	0.647	Fe <sub>78</sub>	0.210
	N <sub>34</sub>	-0.123	N <sub>34</sub>	-0.307	N <sub>34</sub>	0.209
	N <sub>68</sub>	0.554	N <sub>68</sub>	0.686	N <sub>68</sub>	0.585
	O <sub>72</sub>	0.589	O <sub>72</sub>	0.566	O <sub>72</sub>	0.544
	C <sub>31</sub>	0.119	C <sub>31</sub>	-0.149	C <sub>31</sub>	-0.198
	C <sub>65</sub>	-0.298	C <sub>65</sub>	-0.268	C <sub>65</sub>	-0.287

HOMO–LUMO energy gap for Cu(II), Cd(II) and Fe(III) were 1.30, 0.8 and 1.0029 e V, respectively [60–62], and values of HOMO and LUMO was matched with oxidation and reduction of cyclic voltammetry and UV spectrum, From Fig. 11, we notice that the charge distribution of electrons in HOMO and LUMO molecular orbitals in one side for Cu(II) complex, while the distribution of Cd(II) and Fe(III) was mostly of all complex and they have the smallest energy and can easily charge transfer to use further in solar energy batteries [57, 59] (Table 4).

## Conclusion

In this study, the reactivity of carboxymethyl cellulose with thiosemicarbazide in an acidic medium produced 5-amino-1, 3, 4-thiadiazol cellulose derivatives that were confirmed by FT-IR, XRD, and theoretical investigation using the DFT/B3LYP/6-31 level that served as the ligand (HL) and complexed with metals to form Cu(II), Cd(II), and Fe(III) cellulose complex. Also, the structures had greater antibacterial activity and demonstrated greater reactivity of the Cu(II) complex structure when docked with various proteins. Furthermore, cyclic voltammetry was used to examine these metals and their ligands during oxidation and reduction. This method is consistent with theoretical studies that used DFT DFT/ B3PW91/LANDZ2 level of theory, which has the smallest gap between HOMO–LUMO energy gap and is therefore easily capable of electron transfer.

**Acknowledgements** The authors acknowledge the National Research Center (NRC), Egypt.

## Declarations

**Conflict of interest** The authors declare that they have no conflict of interest.

## References

1. E.M. Akl, S. Dacrory, M.S. Abdel-Aziz, S. Kamel, A.M. Fahim, Preparation and characterization of novel antibacterial blended films based on modified carboxymethyl cellulose/phenolic compounds. *Polym. Bull.* **78**, 1061–1085 (2021)
2. M. Duque-Acevedo, L.J. Belmonte-Ureña, F.J. Cortés-García, F. Camacho-Ferre, Agricultural waste: review of the evolution, approaches and perspectives on alternative uses. *Glob. Ecol. Conserv.* **22**, e00902 (2020)
3. A.M. Fahim, E.E. Abu-El Magd, Performance efficiency of MIP OH polymers as organic filler on cellulose pulp waste to form cellulosic paper sheets with biological evaluation and computational studies. *Polym. Bull.* **79**, 4099–4131 (2021)
4. A.M. Fahim, E.E. Abu-El Magd, Enhancement of Molecular imprinted polymer as organic fillers on bagasse cellulose fibers with biological evaluation and computational calculations. *J. Mol. Struct.* **1241**, 130660 (2021)
5. S. Dacrory, S. Kamel, Magnetic composite based on cellulose and GO for latent fingerprint visualization. *Egypt. J. Chem.* **65**, 1–6 (2022)
6. H. Bayrak, A.M. Fahim, F.Y. Karahalil, I. Azafad, G.M. Boyraci, E. Taflan, Synthesis, antioxidant activity, docking simulation, and computational investigation of novel heterocyclic compounds and Schiff bases from picric acid. *J. Mol. Struct.* **1281**, 135184 (2023). <https://doi.org/10.1016/j.molstruc.2023.135184>




7. M. Abdelraof, M.S. Hasanin, M.M. Farag, H.Y. Ahmed, Green synthesis of bacterial cellulose/bioactive glass nanocomposites: effect of glass nanoparticles on cellulose yield, biocompatibility and antimicrobial activity. *Int. J. Biol. Macromol.* **138**, 975–985 (2019)
8. A.M. Fahim, R.E. Abouzeid, S.A. Al Kiey, S. Dacrory, Development of semiconductive foams based on cellulose-benzene-sulfonate/CuFe<sub>2</sub>O<sub>4</sub>-nanoparticles and theoretical studies with DFT/B3PW91/LANDZ2 basis set. *J. Mol. Struct.* **1247**, 131390 (2022)
9. A.H. Hashem, M. Hasanin, S. Kamel, S. Dacrory, A new approach for antimicrobial and antiviral activities of biocompatible nanocomposite based on cellulose, amino acid and graphene oxide. *Colloids Surf. B Biointerfaces* **209**, 112172 (2022)
10. S. Dacrory, A.H. Hashem, S. Kamel, Antimicrobial and antiviral activities with molecular docking study of chitosan/carrageenan@ clove oil beads. *Biotechnol. J.* **17**, 2100298 (2022)
11. M. Hasanin, A. El-Henawy, W.H. Eisa, H. El-Saied, M. Sameeh, Nano-amino acid cellulose derivatives: eco-synthesis, characterization, and antimicrobial properties. *Int. J. Biol. Macromol.* **132**, 963–969 (2019)
12. A. Salama, M. Hasanin, P. Hesemann, Synthesis and antimicrobial properties of new chitosan derivatives containing guanidinium groups. *Carbohydr. Polym.* **241**, 116363 (2020)
13. A. Aboelnaga, E. Mansour, A.M. Fahim, G.H. Elsayed, Synthesis, anti-proliferative activity, gene expression, docking and DFT investigation of novel Pyrazol-1-yl-thiazol-4 (5H)-one derivatives. *J. Mol. Struct.* **1251**, 131945 (2021)
14. A. Asmaa, M.F. Asmaa, H.E.L.S. Taghreed, Computer aid screening for potential antimalarial choroquinone compounds as Covid 19 utilizing computational calculations and molecular docking study. *OnLine J. Biol. Sci.* **20**, 207–220 (2020)
15. H.S. Magar, E.E. Abu-El Magd, R.Y.A. Hassan, A.M. Fahim, Rapid impedimetric detection of cadmium ions using Nanocellulose/ligand/nanocomposite (CNT/Co<sub>3</sub>O<sub>4</sub>). *Microchem. J.* **182**, 107885 (2022). <https://doi.org/10.1016/j.microc.2022.107885>
16. M. Al-Ibrahim, H.-K. Roth, M. Schroedner, A. Konkin, U. Zhokhavets, G. Gobsch, P. Scharff, S. Sensfuss, The influence of the optoelectronic properties of poly(3-alkylthiophenes) on the device parameters in flexible polymer solar cells. *Org. Electron.* **6**, 65–77 (2005)
17. A.M. Fahim, H.S. Magar, N.H. Mahmoud, Synthesis, anti-proliferative activities, docking studies, and computational calculations of novel isonicotinic mixed complexes. *Appl. Organomet. Chem.* **36**(5), e6616 (2022). <https://doi.org/10.1002/aoc.6616>
18. A. Mohamed, A.M. Fahim, M.A. Ibrahim, Theoretical investigation on hydrogen bond interaction between adrenaline and hydrogen sulfide. *J. Mol. Model.* **26**, 1–13 (2020)
19. I.H.I. Habib, H.N.A. Hassan, R. Attar, New alternative cyclic voltammetry for HOMO and LUMO estimation of organic materials. Under preparation for the publication. 2021
20. A. Attia, A. Aboelnaga, A.M. Fahim, Isonicotinohydrazide chalcone base and its Ni complex as corrosion inhibitors during acid cleaning: theoretical and experimental approaches. *Egypt. J. Chem.* (2022). <https://doi.org/10.21608/ejchem.2022.166142.7046>
21. A.M. Fahim, Anti-proliferative activity, molecular docking study of novel synthesized ethoxyphenylbenzene sulfonamide with computational calculations. *J. Mol. Struct.* **1277**, 134871 (2023)
22. A.M. Fahim, H.S. Magar, N.H. Mahmoud, Synthesis, antimicrobial, antitumor activity, docking simulation, theoretical studies, and electrochemical analysis of novel Cd(II), Co(II), Cu(II), and Fe(III) complexes containing barbituric moiety. *Appl. Organomet. Chem.* **2023**, e7023 (2023)
23. F. Josefík, T. Mikysek, M. Svobodová, P. Šimůnek, H. Kvapilová, J. Ludvik, New triazaborine chromophores: their synthesis via oxazaborines and electrochemical and DFT study of their fundamental properties. *Organometallics* **33**, 4931–4939 (2014)
24. D.P. Rillema, S.R. Stayanov, A.J. Cruz, H. Nguyen, C. Moore, W. Huang, K. Siam, A. Jehan, V. KomReddy, HOMO-LUMO energy gap control in platinum(II) biphenyl complexes containing 2,2'-bipyridine ligands. *Dalton Trans.* **44**, 17075–17090 (2015)
25. T. Mikysek, H. Kvapilova, F. Josefík, J. Ludvik, Electrochemical and theoretical study of a new series of bicyclic oxazaborines. *Anal. Lett.* **49**, 178–187 (2016)
26. Inc. CCG, *Molecular Operating Environment (MOE)* (Chemical Computing Group Inc, Montreal, 2016)
27. H.-J. Li, X. Li, N. Liu, H. Zhang, J.J. Truglio, S. Mishra, C. Kisker, M. Garcia-Diaz, P.J. Tonge, Mechanism of the intramolecular Claisen condensation reaction catalyzed by MenB, a crotonase superfamily member. *Biochemistry* **50**, 9532–9544 (2011)
28. G. Hagelueken, H. Huang, I.L. Mainprize, C. Whitfield, J.H. Naismith, Crystal structures of Wzb of *Escherichia coli* and CpsB of *Streptococcus pneumoniae*, representatives of two families of tyrosine phosphatases that regulate capsule assembly. *J. Mol. Biol.* **392**, 678–688 (2009)
29. H. Yoshida, G. Sakai, K. Mori, K. Kojima, S. Kamitori, K. Sode, Structural analysis of fungus-derived FAD glucose dehydrogenase. *Sci. Rep.* **5**, 1–13 (2015)
30. Z. Juo, T. Chiu, P. Leiberman, I. Baikalov, A.J. Berk, R.E. Dickerson, *J. Mol. Biol.* **261**, 239–254 (1996)
31. B.W. D'Andrade, S. Datta, S.R. Forrest, P. Djurovich, E. Polikarpov, M.E. Thompson, Relationship between the ionization and oxidation potentials of molecular organic semiconductor. *Org. Electron.* **6**, 11–20 (2005)
32. P.I. Djurovich, E.I. Mayo, S.R. Forrest, M.E. Thompson, Measurement of the lowest unoccupied molecular orbital energies of molecular organic semiconductors. *Org. Electron.* **10**, 515–520 (2009)
33. Z.-L. Gua, J.B. Kim, H. Wang, C. Jaye, D.A. Fischer, Y.-L. Loo, A. Kahn, Direct determination of the electronic structure of the poly(3-hexylthiophene):phenyl-[66]-C61 butyric acid methyl ester blend. *Org. Electron.* **11**, 1779–1785 (2010)
34. H.B. Schlegel, Optimization of equilibrium geometries and transition structures. *J. Comput. Chem.* **3**, 214–218 (1982)
35. Gaussian JJIWC. 09, revision A. 02 (Gaussian, 2009)
36. A.M. Fahim, A.M. Farag, A. Mermer, H. Bayrak, Y. Şirin, Synthesis of novel β-lactams: antioxidant activity, acetylcholinesterase inhibition and computational studies. *J. Mol. Struct.* **1233**, 130092 (2021)
37. A. Fahim, E. Ismael, Synthesis, antimicrobial activity and quantum calculations of novel sulphonamide derivatives. *Egypt. J. Chem.* **62**, 1427–1440 (2019)
38. A.P. Imeson, *Thickening and Gelling Agents for Food* (Springer, 2012)
39. E.M. Zayed, M.A. Zayed, A.M. Fahim, F.A. El-Samahy, Synthesis of novel macrocyclic Schiff's-base and its complexes having N2O2 group of donor atoms. Characterization and anticancer screening are studied. *Appl. Organomet. Chem.* **31**, e3694 (2017)
40. N.H. Mahmoud, A.A.A. Emara, W. Linert, A.M. Fahim, A.A. Abou-Hussein, Synthesis, spectral investigation, biological activities and docking stimulation of novel metal complexes of Trifluoro phenylthiazol derivative with computational studies. *J. Mol. Struct.* **1272**, 134095 (2023)
41. A.M. Fahim, H.S. Magar, M.A. Ayoub, Synthesis, characterization, thermal studies, electrochemical behavior, antimicrobial, docking studies, and computational simulation of triazole-thiol metal complexes. *Appl. Organomet. Chem.* **36**(5), e6647 (2022). <https://doi.org/10.1002/aoc.6647>
42. S. Dacrory, H. Abou-Yousef, S. Kamel, G. Turkey, Development of biodegradable semiconducting foam based on micro-fibrillated cellulose/Cu-NPs. *Int. J. Biol. Macromol.* **132**, 351–359 (2019)



43. A.M. Fahim, H.A. Ghabbour, M.M. Kabil, S.T. Al-Rashood, H.A. Abdel-Aziz, Synthesis, X-ray crystal structure, Hirshfeld analysis and computational investigation of bis(methylthio)acrylonitrile with antimicrobial and docking evaluation. *J. Mol. Struct.* **1260**, 132793 (2022)
44. P.X. Gao, Y. Ding, W. Mai, W.L. Hughes, C. Lao, Z.L.J.S. Wang, Conversion of zinc oxide nanobelts into superlattice-structured nanohelices. *Science* **309**, 1700–1704 (2005)
45. A. Youssef, M. Hasanin, M. Abd El-Aziz, G.M. Turky, Conducting chitosan/hydroxyethyl cellulose/polyaniline bionanocomposites hydrogel based on graphene oxide doped with Ag-NPs. *Int. J. Biol. Macromol.* **167**, 1435–1444 (2021)
46. M.A. Shalaby, A.M. Fahim, S.A. Rizk, Microwave-assisted synthesis, antioxidant activity, docking simulation, and DFT analysis of different heterocyclic compounds. *Sci. Rep.* **13**, 4999 (2023). <https://doi.org/10.1038/s41598-023-31995-w>
47. H. Abou-Yousef, S. Dacrory, M. Hasanin, E. Saber, S. Kamel, Biocompatible hydrogel based on aldehyde-functionalized cellulose and chitosan for potential control drug release. *Sustain. Chem. Pharm.* **21**, 100419 (2021)
48. S. Dacrory, A.H. Hashem, M. Hasanin, Synthesis of cellulose based amino acid functionalized nano-bio-complex: characterization, antifungal activity, molecular docking and hemocompatibility. *Environ. Nanotechnol. Monit. Manag.* **15**, 100453 (2021)
49. H. Elsayed, M. Hasanin, M. Rehan, Enhancement of multifunctional properties of leather surface decorated with silver nanoparticles (Ag NPs). *J. Mol. Struct.* **1234**, 130130 (2021)
50. S. Vilar, G. Cozza, S. Moro, Medicinal chemistry and the molecular operating environment (MOE): application of QSAR and molecular docking to drug discovery. *CTMC* **8**, 1555–1572 (2008)
51. Y.U. Cebeci, H. Bayrak, Ş.A. Karaoğlu, A.M. Fahim, Synthesis of novel antipyrine-azole-S-alkyl derivatives antimicrobial activity, molecular docking, and computational studies. *J. Mol. Struct.* **1260**, 132810 (2022)
52. J.C. Costa, R.J. Taveira, C.F. Lima, A. Mendes, L.M. Santos, Optical band gaps of organic semiconductor materials. *Opt. Mater.* **58**, 51–60 (2016)
53. A. Frisch. *Gaussian 09W Reference* (Wallingford, 2009).
54. H.A. Ghabbour, A.M. Fahim, M.A. Abu El-Enin, S.T. Al-Rashood, H.A. Abdel-Aziz, Crystal structure, Hirshfeld surface analysis and computational study of three 2-(4-arylthiazol-2-yl) isoindoline-1,3-dione derivatives. *Mol. Cryst. Liq. Cryst.* (2022). <https://doi.org/10.1080/15421406.2022.2045794>
55. A.M. Fahim, M.S. Elshikh, N.M. Darwish, Synthesis, antitumor activity, molecular docking and DFT study of novel pyrimidopyrazole derivatives. *Curr. Comput. Aided Drug Des.* **16**, 486–499 (2020)
56. A.M. Fahim, B. Wasiniak, J.P.C. Łukaszewicz, Molecularly imprinted polymer and computational study of (E)-4-(2-cyano-3-(dimethylamino) acryloyl) benzoic acid from poly(ethylene terephthalate) plastic waste. *CAC* **16**, 119–137 (2020)
57. A.M. Fahim, H.E. Tolan, W.A. El-Sayed, Synthesis of novel 1, 2, 3-triazole based acridine and benzothiazole scaffold N-glycosides with anti-proliferative activity, docking studies, and comparative computational studies. *J. Mol. Struct.* **1251**, 131941 (2021)
58. A.M. Fahim, H.E. Tolan, H. Awad, E.H. Ismael, Synthesis, antimicrobial and antiproliferative activities, molecular docking, and computational studies of novel heterocycles. *J. Iran. Chem. Soc.* (2021). <https://doi.org/10.1007/s13738-021-02251-7>
59. A.M. Fahim, H.S. Magar, E. Nasar, F.M. Abdelrazek, A. Aboelnaga, Synthesis of Cu-porphyrazines by annulated diazepine rings with electrochemical, conductance activities and computational studies. *J. Inorg. Organomet. Polym. Mater.* (2021). <https://doi.org/10.1007/s10904-021-02122-x>
60. G.H. Elsayed, S. Dacrory, A.M. Fahim, Anti-proliferative action, molecular investigation and computational studies of novel fused heterocyclic cellulosic compounds on human cancer cells. *Int. J. Biol. Macromol.* **222**, Part B, 3077–3099 (2022). <https://doi.org/10.1016/j.ijbiomac.2022.10.083>
61. A.M. Fahim, A.M. Farag, Synthesis, antimicrobial evaluation, molecular docking and theoretical calculations of novel pyrazolo [1, 5-a] pyrimidine derivatives. *J. Mol. Struct.* **1199**, 127025 (2020)
62. A.M. Fahim, Microwave assisted regioselective synthesis and biological evaluation of Pyrano[2,3-c]Pyridine derivatives utilizing DMAP as a catalyst. *OnLine J. Biol. Sci.* **17**(4), 394–403 (2017). <https://doi.org/10.3844/ojbsci.2017.394.403>

Springer Nature or its licensor (e.g. a society or other partner) holds exclusive rights to this article under a publishing agreement with the author(s) or other rightsholder(s); author self-archiving of the accepted manuscript version of this article is solely governed by the terms of such publishing agreement and applicable law.

## Authors and Affiliations

Asmaa M. Fahim<sup>1</sup>  · Mohamed Hasanin<sup>2</sup> · I. H. I. Habib<sup>3</sup> · Rehab O. El-Attar<sup>3</sup> · Sawsan Dacrory<sup>2</sup>

<sup>1</sup> Department of Green Chemistry, National Research Centre Dokki, P.O. Box.12622, Cairo, Egypt

<sup>2</sup> Department of Cellulose and Paper, National Research Centre, Giza 12622, Egypt

<sup>3</sup> Microanalysis Laboratory, Applied Organic Chemistry Department, National Research Centre, El-Bohouth St., Dokki, Giza 12622, Egypt